How ATP is used by P-glycoprotein to export multiple hydrophobic compounds

Authors/Affiliations

Ryota Futamata[1], Fumihiko Ogasawara[2], Takafumi Ichikawa[1], Yasuhisa Kimura[1], Noriyuki Kioka[1] and Kazumitsu Ueda[2]

[1]Graduate School of Agriculture, Kyoto University, Kyoto 606-8502, Japan, [2]Institute for integrated Cell-Material Sciences (WPI-iCeMS), KUIAS, Kyoto University, Kyoto 606-8501, Japan

***Corresponding Author**

Kazumitsu Ueda, uedak@kais.kyoto-u.ac.jp

Address: Institute for integrated Cell-Material Sciences (WPI-iCeMS), KUIAS, Kyoto University, Yoshida-honmachi, Sakyo, Kyoto 606-8501, Japan Tel: +81-75-753-9825, Fax: +81-75-753-6104

Abstract

It remains unclear how ATP is used by human P-glycoprotein, a multidrug efflux pump, to extrude various hydrophobic toxic compounds to extracellular space. FRET analysis revealed that binding of two MgATP provides the energy for the conformational change to the rigid outward-facing conformation in living cells. ATP hydrolysis, and subsequent release of γ-phosphate and Mg^{2+} from both NBDs, allows it to return to the original inward-facing conformation.

Main text

P-glycoprotein (P-gp; also known as MDR1 or ABCB1), a member of the ATP-binding cassette (ABC) transporter family, is an ATP-dependent efflux pump that transports various hydrophobic compounds[1,2]. Its substrates include therapeutic drugs, alkaloids, flavonoids, and other hydrophobic natural toxic compounds. P-gp is an essential component of protective physiological barriers in important organs[3], such as brain and testis. The protein consists of four core domains: two transmembrane domains (TMDs), which create the translocation pathway for substrates, and two nucleotide-binding domains (NBDs), which bind and hydrolyze ATP to power the transport process. Although numerous studies were conducted[4-8] following the discovery of P-gp[9-11], it remains unclear how ATP is utilized by P-gp to export hydrophobic compounds from cells.

Recently, we reported a pair of structures of the P-gp orthologue (CmABCB1) from the thermophilic unicellular eukaryote *Cyanidioschyzon merolae*, in the inward-facing apo state[12] and outward-facing state with bound nucleotide[13], at resolutions of 2.4 Å and 1.9 Å, respectively. Conformational changes from the inward-facing to the outward-facing state could be clearly visualized at these high resolutions. Conformational change in the NBDs caused by MgATP binding mediates TMD movements via NBD–TMD interactions, which is aided by a relay of van der Waals interactions among the side chains of residues in the helical sub-domain of the NBD, coupling helices, and TM helices. These results suggest that MgATP binding in both NBDs drives conformational movements from the inward-facing to the rigid outward-facing conformation of P-gp,

and that ATP hydrolysis releases the conformation from the outward-facing state to the inward-facing state. However, a recent double electron–electron resonance (DEER) study of purified mouse P-gp suggested that ATP hydrolysis in one NBD powered isomerization of P-gp from the inward-facing to the outward-facing conformation[14]. Consequently, the role of ATP hydrolysis in conformational movements of P-gp remains unclear. In this study, we examined the role of ATP binding and hydrolysis in conformational movements of human P-gp in intact living cells and permeabilized semi-intact cells.

To detect conformational changes of human P-gp in living cells in real time, we generated four constructs: P-gp–FRET; P-gp–VsCn (as a positive control); P-gp–Cerulean and P-gp–Venus (as negative controls) (Fig. 1a). When these constructs were transiently expressed in HEK293 cells, the expected fluorescence signals were observed on the plasma membrane (Supplementary Fig. 1a). Weak and strong signals were observed in the FRET channel with P-gp–FRET and P-gp–VsCn, respectively, whereas almost no signal was observed with P-gp–Cerulean or P-gp–Venus (Supplementary Fig. 1a, the right end panels). When cells expressing these P-gp constructs were incubated with rhodamine 6G (R6G), a substrate for P-gp, R6G accumulated to a lower level than in mock-transfected cells; R6G accumulation was restored by co-incubation with PSC-833, a specific inhibitor of P-gp (Supplementary Fig. 1b). These results indicated that neither insertion nor fusion of fluorescent proteins impaired the plasma membrane localization or function of P-gp.

Next, we investigated whether the addition of a transport substrate would affect FRET efficiency (eFRET). eFRET was defined as the ratio of the corrected intensity of FRET signal divided by the Cerulean intensity, which is shown in pseudocolor in Fig. 1b. The FRET signal of P-gp–FRET on the plasma membrane (shown in green) was low, and the signal of P-gp–VsCn (shown in yellow or red) was high. When verapamil, a transport substrate of P-gp[15] that stimulates its ATPase activity (Supplementary Fig. 2), was added to cells, the plasma membrane of P-gp–FRET expressing cells turned yellow or red from green, whereas that of P-gp–VsCn was unchanged (Fig. 1b). Thus, eFRET of P-gp–FRET was increased by the addition of verapamil. eFRET was not affected by the expression level of P-gp (Supplementary Fig. 3b), suggesting that intermolecular FRET did not occur. eFRET of P-gp–FRET increased about 1.5-fold upon addition of 100 μM verapamil, close to the level of P-gp–VsCn (Fig. 1c). Verapamil increased eFRET in a concentration dependent manner (Fig. 1d). The EC_{50} was 3.9 ± 0.9 μM, comparable to the K_M (2.2 ± 0.2 – 4.1 ± 0.4 μM) of verapamil-induced ATP hydrolysis of purified human P-gp[16], suggesting that the observed increase in eFRET was caused by conformational changes during substrate transport. On the other hand, eFRET of P-gp–VsCn was not affected by the addition of verapamil, and that of P-gp–Cerulean was less than one-tenth that of P-gp–VsCn. These results suggest that verapamil causes conformational changes, which allow Cerulean inserted after NBD1 and Venus fused after NBD2 to approach each other in close enough proximity, via dimerization of the two NBDs, to increase intramolecular FRET. This is consistent with the prediction that transport substrates trigger a conformational change from

the inward-facing to the outward-facing structure by interacting with the tight van der Waals network among the aromatic and hydrophobic residues at the ceiling of the inner chamber of the inward-facing structure, thereby destabilizing it[12].

To investigate the involvement of ATP binding and ATP hydrolysis in the conformational change induced by verapamil, we constructed P-gp(MM)–FRET, in which conserved lysine residues in the Walker A motif crucial for ATP binding[8,13,17] were replaced by methionines, and P-gp(QQ)–FRET, in which glutamate residues in the Walker B motif crucial for ATP hydrolysis[13,18] were replaced by glutamines. Both P-gp(MM)–FRET and P-gp(QQ)–FRET properly localized to the plasma membrane (Supplementary Fig. 4a) but had no R6G transport activity (Supplementary Fig. 4b). eFRET of P-gp(MM)–FRET was comparable to that of P-gp–FRET without verapamil and was not increased by verapamil (Fig. 2a). On the other hand, eFRET of P-gp(QQ)–FRET was significantly higher than that of P-gp–FRET in the absence of verapamil and was not increased by verapamil (Fig. 2b). Like P-gp–VsCn, control constructs P-gp(MM)–VsCn and P-gp(QQ)–VsCn exhibited high eFRET in the absence or presence of verapamil. These results suggest that ATP binding is required for the conformational change of P-gp induced by verapamil.

To further demonstrate the role of ATP binding in the conformational change of P-gp, cells were moderately permeabilized by 50 ng/mL streptolysin O (SLO) in order to deplete intracellular ATP. 4',6-diamidino-2-phenylindole (DAPI)-positive cells, whose plasma membranes were permeabilized, were used for FRET analysis (Supplementary Fig. 5). DAPI is not a transport substrate of P-gp and

does not stimulate its ATPase activity (Supplementary Fig. 2). In the presence of exogenously added MgATP, eFRET of P-gp–FRET was increased by the addition of verapamil (Fig. 2c), as in intact cells (Fig. 2a). However, in the absence of MgATP, eFRET of P-gp–FRET was not increased even after addition of verapamil. eFRET of P-gp(QQ)–FRET was high in the presence of exogenously added MgATP, even without verapamil, but low in the absence of MgATP (Fig. 2d). These results suggest that MgATP binding is prerequisite for the conformational change of P-gp.

Next, to investigate the role of ATP hydrolysis in the conformational change of P-gp, we incubated ATP-depleted cells with the nonhydrolyzable ATP analogue adenylyl-imidodiphosphate (AMP-PNP) (Fig. 2e). In the presence of exogenously added MgAMP-PNP, P-gp–FRET exhibited eFRET as high as P-gp–VsCn even without verapamil. This suggests that human P-gp moves spontaneously between the inward-facing and outward-facing structures, and that the non-hydrolysable ATP stabilizes dimerized NBD and fixes P-gp to the outward-facing structure, even though P-gp is predicted to be more stable in the inward-facing structure than in the outward-facing structure[13], which is likely short-lived and rare. When cells were incubated with MgATP and sodium orthovanadate, which traps P-gp in the stable post-hydrolysis transition state[19,20], P-gp–FRET also exhibited high eFRET (Fig. 2e). These results suggest that ATP hydrolysis and subsequent release of γ-phosphate reset the conformation of P-gp to the low FRET state, consistent with results obtained using a range of techniques, including cryo-EM[8], luminescence[7], and antibody binding[6]. Single Walker B glutamate mutants, P-gp(QE)–FRET and P-gp(EQ)–FRET, which had no R6G transport

activity (Supplementary Fig. 6b), exhibited high eFRET in living cells (Fig. 2f). These observations suggest that ATP hydrolysis and subsequent release of γ-phosphate in both NBDs are required for the return to the inward-facing conformation, as illustrated in Fig. 3. By contrast, other studies have reported that AMP-PNP does not cause conformational changes of P-gp[5,14] and that ATP does not cause conformational changes of the Walker B glutamate mutant[14]; these observations suggest that ATP hydrolysis causes a transition from the inward-facing to the outward-facing structure[5,14]. However, because those experiments were performed under a non-native membrane environment, in contrast to our study, they might not reflect the behavior of P-gp in living cells. Furthermore, Verhalen et al. predicted the outward-facing conformation modeled on the bacterial homolog MsbA[14], whose outward-facing structure has a large inner chamber that opens into the plasma membrane; this is not the case for human P-gp[8] and CmABCB1[13].

It is hard to explain the extrusion of various hydrophobic compounds in terms of the conventional alternating access model proposed by Jardetzky[21], in which exporters are predicted to have a high-affinity specific binding site for substrates in the inward-facing conformation and a low-affinity binding site in the outward-facing conformation. Consequently, exporters cannot recognize substrates with various structures, and hydrophobic substrates will not diffuse into the extracellular hydrophilic space via Brownian motion from the outward-facing binding site. Alternatively, it has been proposed that substrates for P-gp interact with low affinity with the surface residues of the large inner cavity[12] and are directly extruded to the extracellular hydrophilic space by

contraction of the inner cavity[13]. It has been predicted that a relay of van der Waals interactions and hydrogen-bond networks formed by ATP binding propagate from the NBDs to the whole molecule, and that the TMDs are shifted to the rigid body. The inner chamber contracts, the substrate-binding cavity collapses, and the substrate has to move outward, and is thus directly expelled into the extracellular space. This mechanism has been also proposed for ABCG2[22]. In CmABCB1, Mg^{2+} is bound in optimal octahedral coordination, with 2.0–2.1 Å bonds formed with oxygens including those from the β- and γ-phosphates of ATP. It is likely that Mg^{2+} bound to unhydrolyzed ATP provides the energy for the conformational change to the rigid outward-facing conformations. The pairing between glutamate and arginine at the bottom of the NBDs, which allows the formation of a salt bridge, stabilizes the outward-facing conformation until the substrate is expelled[13]. Our FRET analysis supports the idea that binding of two MgATP provides the energy for the conformational change of P-gp to the rigid outward-facing conformation, allowing it to expel various hydrophobic substrates from living cells. ATP hydrolysis and subsequent release of γ-phosphate from both NBDs allows it to return to the original inward-facing conformation. (1763 words)

Main Figure legends

Figure 1. Effect of a transport substrate on conformational changes of P-gp.

(**a**) Schematic representations of fluorescent protein–tagged P-gps. (**b**) eFRET pseudocolor images of HEK293 cells expressing fluorescent protein–tagged P-gps. Cells were treated with DMSO or 100 μM verapamil for 5 min at 37°C. eFRET is shown in 8-color scales; each of these hues has a range of 32 intensities based on the corrected intensity of the FRET image. Scale bar; 10 μm. (**c**) Quantification of eFRET. The area corresponding to the plasma membrane was determined from automatically segmented Venus or Cerulean images (Supplementary Fig. 3a), and then eFRET on the plasma membrane was calculated. (**d**) Dose-dependent increase of eFRET by verapamil. All eFRET values are shown relative to that of P-gp–VsCn. Data are expressed as means ± S.E.; n = 10–15 cells per sample; ***$P < 0.001$; N.S., $P > 0.05$. P-gp–FRET exhibited a significant level of eFRET even in the absence of verapamil or MgATP. It is likely that weak FRET occurred even in the inward-facing conformation because the two NBDs separate about 30 Å[4, 14], which is close enough for energy transfer.

Figure 2. Effects of ATP binding and ATP hydrolysis on conformational changes of P-gp

(**a,b**) eFRET in intact cells of the ATP binding–deficient mutant MM (**a**) and ATP hydrolysis–deficient mutant QQ (**b**). HEK293 cells transiently transfected with fluorescent

protein–tagged P-gps were treated with DMSO (empty) or 100 μM verapamil (blue) for 5 min at 37°C. (**c,d**) eFRET in permeabilized semi-intact cells treated with DMSO (empty) or 100 μM verapamil (blue) in the presence or absence of 4.5 mM MgATP (hatched). (**e**) eFRET in permeabilized semi-intact cells in the presence of 4.5 mM MgATP (empty) or 4.5 mM MgAMP-PNP (magenta) or 4.5 mM MgATP and 1 mM orthovanadate (green). (**f**) eFRET in intact cells of single Walker B mutants, QE and EQ. All eFRET values are shown relative to that of P-gp–VsCn. Data are expressed as means ± S.E.; n = 12–15 cells per sample; **P < 0.01; ***P < 0.001; N.S., P > 0.05.

Figure 3. Schematic illustration of ATP-dependent conformational changes of P-gp

Inward-facing conformation is stable in the absence of transport substrate (left). Both transport substrate and MgATP binding cause the transition from the inward-facing to the outward-facing conformation (right). ATP hydrolysis and subsequent release of γ-phosphate from both NBDs allow P-gp to return to the inward-facing state. Mutation of the Walker A lysine prevents ATP binding. Mutation of the Walker B glutamate or binding of MgAMP-PNP inhibits ATP hydrolysis. Orthovanadate traps P-gp in the stable post–ATP hydrolysis transition state. Cerulean (PDB:2wso) and Venus (PDB: 1myw) were docked with the inward-facing conformation of mouse P-gp (PDB: 4m1m) or the outward-facing conformation of human P-gp (PDB: 6c0v).

References

1 Ueda, K., Cardarelli, C., Gottesman, M. M. & Pastan, I. Expression of a full-length cDNA for the human "MDR1" gene confers resistance to colchicine, doxorubicin, and vinblastine. *Proc Natl Acad Sci U S A* **84**, 3004-3008 (1987).

2 Gottesman, M. M. & Ling, V. The molecular basis of multidrug resistance in cancer: the early years of P-glycoprotein research. *FEBS Lett* **580**, 998-1009, doi:10.1016/j.febslet.2005.12.060 (2006).

3 Schinkel, A. H. *et al*. Disruption of the mouse mdr1a P-glycoprotein gene leads to a deficiency in the blood-brain barrier and to increased sensitivity to drugs. *Cell* **77**, 491-502 (1994).

4 Li, J., Jaimes, K. F. & Aller, S. G. Refined structures of mouse P-glycoprotein. *Protein Sci* **23**, 34-46, doi:10.1002/pro.2387 (2014).

5 Moeller, A. *et al.* Distinct conformational spectrum of homologous multidrug ABC transporters. *Structure* **23**, 450-460, doi:10.1016/j.str.2014.12.013 (2015).

6 Bársony, O. *et al.* A single active catalytic site is sufficient to promote transport in P-glycoprotein. *Sci Rep* **6**, 24810, doi:10.1038/srep24810 (2016).

7 Zoghbi, M. E. *et al.* Substrate-induced conformational changes in the nucleotide-binding domains of lipid bilayer-associated P-glycoprotein during ATP hydrolysis. *J Biol Chem* **292**, 20412-20424, doi:10.1074/jbc.M117.814186 (2017).

8 Kim, Y. & Chen, J. Molecular structure of human P-glycoprotein in the ATP-bound, outward-facing conformation. *Science*, doi:10.1126/science.aar7389 (2018).

9 Juliano, R. L. & Ling, V. A surface glycoprotein modulating drug permeability in Chinese hamster ovary cell mutants. *Biochim Biophys Acta* **455**, 152-162 (1976).

10 Chen, C. J. *et al.* Internal duplication and homology with bacterial transport proteins in the mdr1 (P-glycoprotein) gene from multidrug-resistant human cells. *Cell* **47**, 381-389 (1986).

11 Ueda, K. *et al.* The mdr1 gene, responsible for multidrug-resistance, codes for P-glycoprotein. *Biochem Biophys Res Commun* **141**, 956-962 (1986).

12 Kodan, A. *et al.* Structural basis for gating mechanisms of a eukaryotic P-glycoprotein homolog. *Proc Natl Acad Sci U S A* **111**, 4049-4054, doi:10.1073/pnas.1321562111 (2014).

13 Kodan, A. *et al.* Inward- and outward-facing X-ray crystal structures of homodimeric P-glycoprotein CmABCB1. *Nat Commun* **10**, 88, doi:10.1038/s41467-018-08007-x (2019).

14 Verhalen, B. *et al.* Energy transduction and alternating access of the mammalian ABC transporter P-glycoprotein. *Nature* **543**, 738-741, doi:10.1038/nature21414 (2017).

15 Kimura, Y. *et al.* ATP hydrolysis-dependent multidrug efflux transporter: MDR1/P-glycoprotein. *Curr Drug Metab* **5**, 1-10 (2004).

16 Kimura, Y., Kioka, N., Kato, H., Matsuo, M. & Ueda, K. Modulation of drug-stimulated ATPase activity of human MDR1/P-glycoprotein by cholesterol. *Biochem J* **401**, 597-605, doi:10.1042/BJ20060632 (2007).

17 Szabó, K. *et al.* Drug-stimulated nucleotide trapping in the human multidrug transporter MDR1. Cooperation of the nucleotide binding domains. *J Biol Chem* **273**, 10132-10138 (1998).

18 Tombline, G., Bartholomew, L. A., Urbatsch, I. L. & Senior, A. E. Combined mutation of catalytic glutamate residues in the two nucleotide binding domains of P-glycoprotein generates a conformation that binds ATP and ADP tightly. *J Biol Chem* **279**, 31212-31220, doi:10.1074/jbc.M404689200 (2004).

19 Urbatsch, I. L., Sankaran, B., Weber, J. & Senior, A. E. P-glycoprotein is stably inhibited by vanadate-induced trapping of nucleotide at a single catalytic site. *J Biol Chem* **270**, 19383-19390 (1995).

20 Urbatsch, I. L., Tyndall, G. A., Tombline, G. & Senior, A. E. P-glycoprotein catalytic mechanism: studies of the ADP-vanadate inhibited state. *J Biol Chem* **278**, 23171-23179, doi:10.1074/jbc.M301957200 (2003).

21 Jardetzky, O. Simple allosteric model for membrane pumps. *Nature* **211**, 969-970 (1966).

22 Manolaridis, I. *et al.* Cryo-EM structures of a human ABCG2 mutant trapped in ATP-bound and substrate-bound states. *Nature* **563**, 426-430, doi:10.1038/s41586-018-0680-3 (2018).

23 Iram, S. H., Gruber, S. J., Raguimova, O. N., Thomas, D. D. & Robia, S. L. ATP-Binding Cassette Transporter Structure Changes Detected by Intramolecular Fluorescence Energy

Transfer for High-Throughput Screening. *Mol Pharmacol* **88**, 84-94, doi:10.1124/mol.114.096792 (2015).

24 Ogasawara, F. *et al*. Changes in the asymmetric distribution of cholesterol in the plasma membrane influence streptolysin O pore formation. *Sci Rep* **9**, 4548, doi:10.1038/s41598-019-39973-x (2019).

25 Ishigami, M. *et al*. ATPase activity of nucleotide binding domains of human MDR3 in the context of MDR1. *Biochim Biophys Acta* **1831**, 683-690, doi:10.1016/j.bbalip.2012.12.016 (2013).

26 Kimura, Y. *et al*. Microanalysis for MDR1 ATPase by high-performance liquid chromatography with a titanium dioxide column. *Anal Biochem* **326**, 262-266, doi:10.1016/j.ab.2003.12.012 (2004).

Acknowledgements

This work was supported by JSPS KAKENHI Grant Number 18H05269 to KU and 18K19176 to YK.

Author Contributions

R.F. and K.U. planned the experiments. R.F. conducted the experiments. F.O. and T.I. assisted Data analysis. R.F. and K.U. wrote the paper on the basis of discussions with F.O., Y.K., and N.K. All authors approved the final manuscript.

Additional Information

Supplementary information accompanies this paper.

Competing Interests: The authors declare no competing financial or non-financial interests.

Materials and Methods

Plasmid construction

P-gp constructs were designed as MRP1 FRET constructs[23]. pcDNA3.1P-gp was constructed by the insertion of cDNA encoding human P-gp in pcDNA3.1 (Thermo Fisher Scientific, Austin, TX, USA). To engineer P-gp–Venus, pcDNA3.1(-)P-gp backbone and Venus cDNA were PCR-amplified using primer pairs #1/#2 and #3/#4, respectively. To engineer P-gp–Cerulean, pcDNA3.1(+)P-gp backbone, Cerulean cDNA, and a ten–amino acid linker (GS repeats) were PCR amplified using primer pairs #5/#6 and #7/#8, respectively. The P-gp–FRET construct was generated by inserting Cerulean cDNA and the ten–amino acid linker into pcDNA3.1(-)P-gp–Venus using primer pairs #5/#6 and #7/#8. To engineer P-gp–VsCn, pcDNA3.1(-)P-gp–Venus backbone and Cerulean cDNA were PCR-amplified using primer pairs using #1/#4 and #9/#10, respectively. The amplified fragments were ligated using an In-Fusion HD cloning kit (Clontech, Mountain View, CA, USA). pcDNA3.1(-)P-gp(MM; K433M/K1076M)-FRET and pcDNA3.1(-)P-gp(QQ; E556Q/E1201Q) and other mutants were generated using the corresponding pcDNA3.1(-)P-gp mutant backbones.

Primers:
#1. 5’- TGAGGATCCGAGCTCGGTAC -3’
#2. 5’- CTGGCGCTTTGTTCCAGCCTGGACACTGACCATTG -3’
#3. 5’- GGAACAAAGCGCCAGGTGAGCAAGGGCGAGGAG -3’
#4. 5’- GAGCTCGGATCCTCACTTGTACAGCTCGTCCATG -3’
#5. 5’- TGCTGTCTGCATTGTGACAAGTTTGAAGTAAATGCC -3’
#6. 5’- CAGGTTCTGGCTCAGGCTCTGGATCAGGAAATGAAG -3’

#7. 5’-ACAATGCAGACAGCAGTGAGCAAGGGCGAGGAG-3’
#8. 5’-CTGAGCCAGAACCTGATCCCTTGTACAGCTCGTCC-3’
#9. 5’-GACGAGCTGTACAAGGTGAGCAAGGGCGAGGAGC-3’
#10.5’-GAGCTCGGATCCTCACTTGTACAGCTCGTCCATGC-3’

Flow cytometry

HEK293 cells were cultured in Dulbecco’s modified Eagle’s medium (DMEM; Nacalai Tesque, Kyoto, Japan) supplemented with 10% fetal bovine serum (FBS; Gibco/Thermo) at 37°C under 5% CO_2. HEK293 cells were seeded in 6-well plates (3.0×10^5 cells/well) coated with poly-L-lysine (Sigma-Aldrich, St. Louis, MO, USA) and incubated for 24 h. P-gp constructs were transfected using Lipofectamine LTX Reagent (Thermo Fisher Scientific), and the transfected cells were incubated for an additional 24 h. Medium was replaced with serum-free DMEM containing 1 μM R6G, with or without 25 μM PSC-833, a P-gp inhibitor (Abcam, Cambridge, MA, USA) and incubated for 30 min at 37°C under 5% CO_2. Cells were washed twice with phosphate-buffered saline (PBS). After harvesting, the cells were washed with Hank’s balanced salt solution (HBSS; Gibco) and resuspended in HBSS. R6G accumulation was analyzed on an Accuri C6 flow cytometer (BD Biosciences, Franklin Lakes, NJ, USA).

FRET microscopy

HEK293 cells were seeded at 3.0×10^5 cells/well on glass-bottom dishes (AGC TECHNO GLASS, Shizuoka, Japan) coated with poly-L-lysine and incubated for 24 h. P-gp constructs were transfected using Lipofectamine LTX Reagent, and incubated for an additional 23 h. Medium was then replaced

by Fluoro Brite DMEM supplemented with 10% FBS, sodium pyruvate (Gibco), and GlutaMAX (Gibco) and incubated for another 1 h. Cells were further incubated with 100 μM verapamil chloride (Fujifilm Wako Pure Chemical Corporation, Osaka, Japan) for 5 min at 37°C under 5% CO_2 as necessary. Fluorescence images were acquired at 37°C under 5% CO_2 by an LSM700 confocal microscope equipped with a Plan-Apochromat 63×/1.4 NA oil immersion objective lens (Carl Zeiss, Oberkochen, Germany). Cerulean was excited at 445 nm, and fluorescence emission was collected using a short-pass filter (~490 nm). Venus was excited at 488 nm, and fluorescence emission was collected using a band-pass filter (521–600 nm). For the FRET signal, the laser was set to 445 nm, and sensitized emission was collected using a band-pass filter (521–600 nm).

Cell permeabilization

HEK293 cells were plated at 3.0×10^5 cells/well on glass-bottom based dishes coated with poly-L-lysine and incubated for 24 h. P-gp constructs were transfected using Polyethyleneimine "Max" (MW: 40,000) (PEI-MAX; Polysciences, Warrington, PA, USA) and incubated for an additional 24 h. Cell permeabilization was performed as described previously[24] with slight modifications. Briefly, cells were washed twice with ice-cold PBS and incubated in serum-free DMEM containing 50 ng/μL SLO (BioAcademia, Osaka, Japan) for 5 min on ice, followed by three washes with ice-cold PBS. The cells were further incubated for 10 min at 37°C under 5% CO_2in transport buffer (25 mM HEPES-KOH [pH 7.4], 115 mM KOAc, 4.5 mM $MgCl_2$) preincubated at

37°C containing 2 μg/mL DAPI (Sigma-Aldrich) in the presence or absence of 5 mM ATP disodium salt (Oriental Yeast, Tokyo, Japan). The cells were then washed twice with transport buffer and soaked in transport buffer pre-incubated at 37°C supplemented with 5 mM ATP disodium salt or 5mM AMP-PNP lithium salt (Sigma-Aldrich) or 5 mM ATP disodium salt and 1 mM orthovanadate (Fujifilm Wako), as indicated. The cells were then incubated with 100 μM verapamil chloride for 5 min at 37°C under 5% CO_2 as indicated. Only DAPI-positive cells used for FRET microscopy. FRET microscopy was performed on an LSM700 microscope as described above.

FRET calculation

FRET efficiency (eFRET) was calculated as follows:

$$\mathrm{eFRET} = \frac{I_{DA} - aI_{AA} - dI_{DD}}{I_{DD}}$$

where I_{DA} is the FRET signal or the sensitized emission of the acceptor during donor excitation (Ex 445 nm/Em 521–600 nm), I_{DD} is the donor fluorescence during donor excitation (Ex 445 nm/ Em ~490 nm), and I_{AA} is the acceptor fluorescence during acceptor excitation (Ex 488 nm/Em 521–600 nm). a and d are the crosstalk coefficients of acceptor and donor, respectively. These constants were calculated from P-gp–Venus and P-gp–Cerulean samples using the ImageJ plugin “FRET and Colocalization Analyzer”. eFRET pseudocolour images were generated using the MetaMorph software (Molecular Devices, San Jose, CA, USA). For quantification of eFRET, the plasma membrane was determined from automatically segmented Venus images of P-gp–Venus, P-gp–FRET,

and P-gp–VsCn or Cerulean images of P-gp–Cerulean using the ImageJ-based Fiji software. eFRET was quantified on a cell-by-cell basis.

Protein expression and purification

Human P-gp cDNA was inserted into the expression vector pcDNA3.1(-). The C-terminus of the DNA was modified by elimination of the natural termination codon and insertion of a *Not*I restriction cleavage site, TEV protease cleavage site (ENLYFQG), ten histidine codons, a six–amino acid linker (GAAGTS), and the FLAG tag (DYKDDDDK), followed by a termination codon. FreeStyle 293-F cells (Thermo) were transfected with the resultant P-gp construct using PEI-MAX. After 48 h of transfection, cells were harvested and resuspended in buffer A (50 mM HEPES-Na [pH 7.2], 150 mM NaCl, 50 mM KCl, 20% glycerol) containing 0.5 μM 2-mercaptethanol (Fujifilm Wako) and protease inhibitor (Roche, Basel, Switzerland) and solubilized with 0.6% (w/v) *n*-dodecyl-*β*-D-maltopyranoside (DDM; Anatrace, Maumee, OH). Solubilized proteins were applied to FLAG-M2 agarose (Sigma-Aldrich) pre-equilibrated with buffer A. The mixture was rotated for 18 h. The resin was washed with a 4× bed volume of buffer A containing 0.6% DDM three times. The resin was further washed with 4× bed volume of buffer A containing 0.1% DDM three times. The protein was eluted from the resin with 1× bed volume of buffer A containing 0.1% DDM, 300 μg/mL FLAG peptide (Sigma-Aldrich), and 3× FLAG peptide (Sigma-Aldrich). The eluate was

concentrated by centrifugation using an Amicon Ultra (Merck, Kenilworth, NJ, USA). Purified protein was stored at -80°C. All purification steps were performed at 0–4°C.

Reconstitution into proteoliposomes and measurement of ATPase activity

Purified protein was reconstituted in lipid as described previously[25] with some modifications. Briefly, L-α-lecithin from egg yolk (Fujifilm Wako) was resuspended in reaction buffer (50 mM Tris-HCl (pH7.4), 0.1 mM EGTA) at a final concentration of 20 mg/mL. The suspension was sonicated in a bath sonicator. The purified protein (2.1 μg) was mixed with 40 μg lipid, and the mixture was incubated on ice for 20 min. Proteoliposomes were incubated at 37°C for 30 min with 3 mM ATP disodium salt, 5 mM $MgCl_2$ in 20 μL reaction buffer. Verapamil chloride, DAPI, and BeFx were added to the reaction buffer at 100 μM, 2 μg/mL, and 1 mM, respectively. ATPase reaction was stopped by addition of 20 μL of 20 mM EDTA. ATPase activity was estimated by measuring the amount of released ADP by HPLC using a titanium column[26].

Statistical analysis

Data are presented as means ± S.E.. Multiple comparisons were evaluated using Tukey's post hoc test following one-way ANOVA. All statistical analyses were performed using the Origin2018 software (OriginLab, Massachusetts, USA).

Supplementary Figure Legends

Supplementary Figure 1. Insertion and fusion of fluorescent proteins does not impair the localization or function of P-gp. (**a**) Fluorescent protein–tagged P-gps were transiently expressed in HEK293 cells. Fluorescence images were obtained at 37°C using an LSM700 confocal microscope (Zeiss). Scale bar; 10 μm. (**b**) HEK293 cells transiently expressing fluorescent protein–tagged P-gps were incubated with 1 μM R6G with or without 25 μM inhibitor (PSC-833) for 30 min at 37°C. R6G accumulation in cells was measured by flow cytometry. Due to the leakage of Venus fluorescence in the detection channel, the fluorescence of cells expressing P-gp constructs containing Venus were shifted to the right.

Supplementary Figure 2. Verapamil, a transport substrate, stimulated ATPase activity of P-gp, but DAPI, not a transport substrate, did not. Purified human P-gp was reconstituted in liposomes consisting of L-α-lecithin from egg yolk. Proteoliposomes were incubated for 30 min at 37°C with 3 mM ATP, 5 mM Mg^{2+}, 100 μM verapamil chloride, 2 μg/mL DAPI, and an inhibitor 1 mM beryllium fluoride (BeFx, an ATPase inhibitor). ATPase activity was estimated by measuring the amount of released ADP. Data are expressed as means ± S.E..

Supplementary Figure 3. (**a**) The region of the plasma membrane determined from automatically segmented Venus images of P-gp–FRET and Cerulean images of P-gp–Cerulean. Scale bar; 5 μm. (**b**) Protein expression level had no significant effect on eFRET of P-gp–FRET.

Supplementary Figure 4. (**a**) Subcellular localization and FRET of P-gp(MM)–FRET and P-gp(QQ)–FRET. (**b**) R6G transport activity.

Supplementary Figure 5. Subcellular localization of P-gp–Venus and DAPI staining in cells permeabilized with 50 ng/mL SLO. Fluorescence images were obtained at 37°C on a Nikon C2 confocal system equipped with a Plan Apochromat 40×/ dry objective lens. Scale bar; 10 μm.

Supplementary Figure 6. Subcellular localization and FRET of P-gp(QE)–FRET and P-gp(EQ)–FRET. (**b**) R6G transport activity.

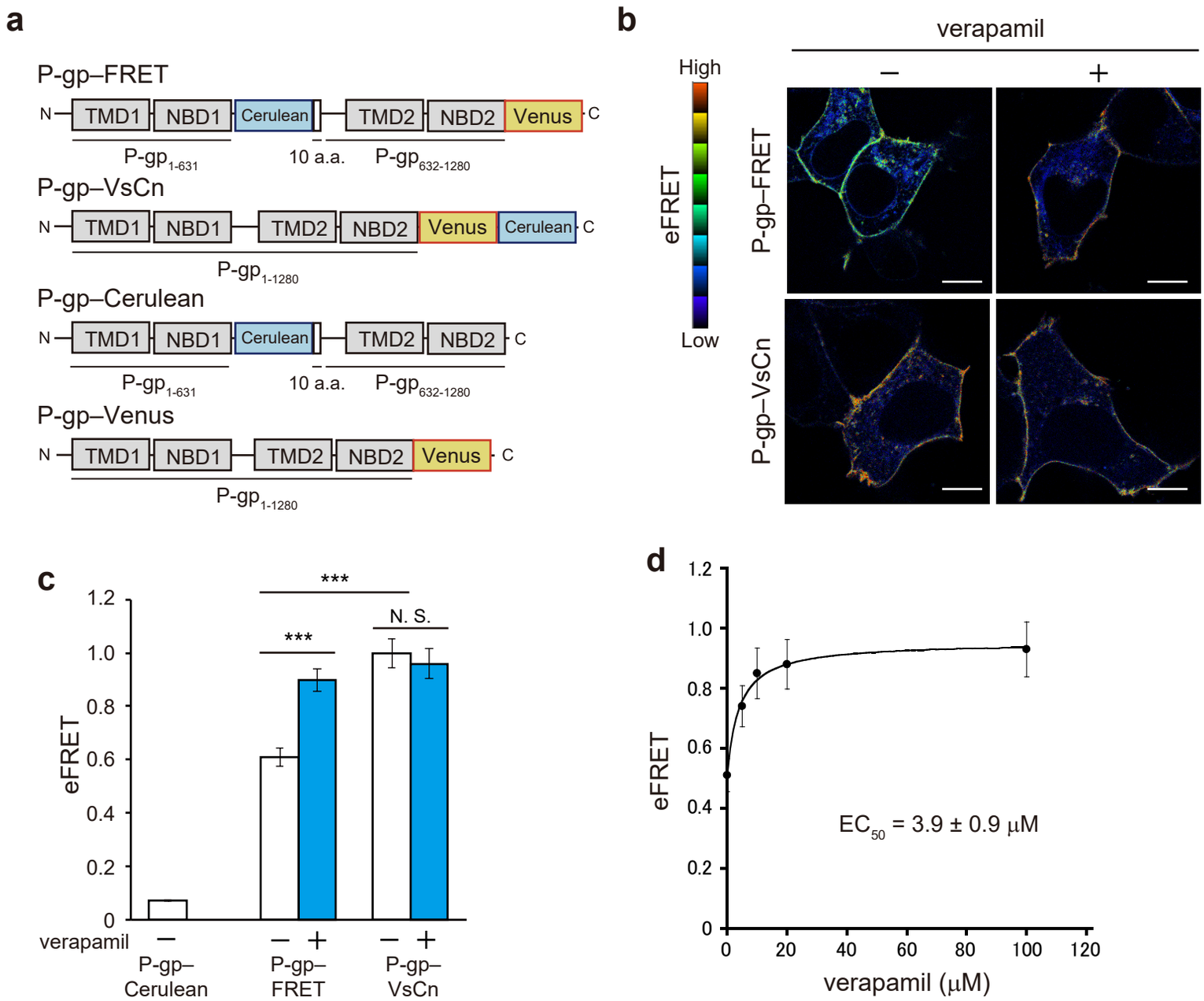
a
P-gp–FRET
N
TMD1
NBD1
Cerulean
TMD2
NBD2
Venus
C
P-gp1-631
10 a.a.
P-gp632-1280
P-gp–VsCn
N
TMD1
NBD1
TMD2
NBD2
Venus
Cerulean
C
P-gp1-1280
P-gp–Cerulean
N
TMD1
NBD1
Cerulean
TMD2
NBD2
C
P-gp1-631
10 a.a.
P-gp632-1280
P-gp–Venus
N
TMD1
NBD1
TMD2
NBD2
Venus
C
P-gp1-1280
b
verapamil
–
+
High
eFRET
Low
P-gp–FRET
P-gp–VsCn
c
1.2
1.0
0.8
0.6
0.4
0.2
0
eFRET
***
***
N. S.
verapamil
–
–
+
–
+
P-gp–Cerulean
P-gp–FRET
P-gp–VsCn
d
1.2
1.0
0.8
0.6
0.4
0.2
0
eFRET
EC50 = 3.9 ± 0.9 μM
0
20
40
60
80
100
120
verapamil (μM)

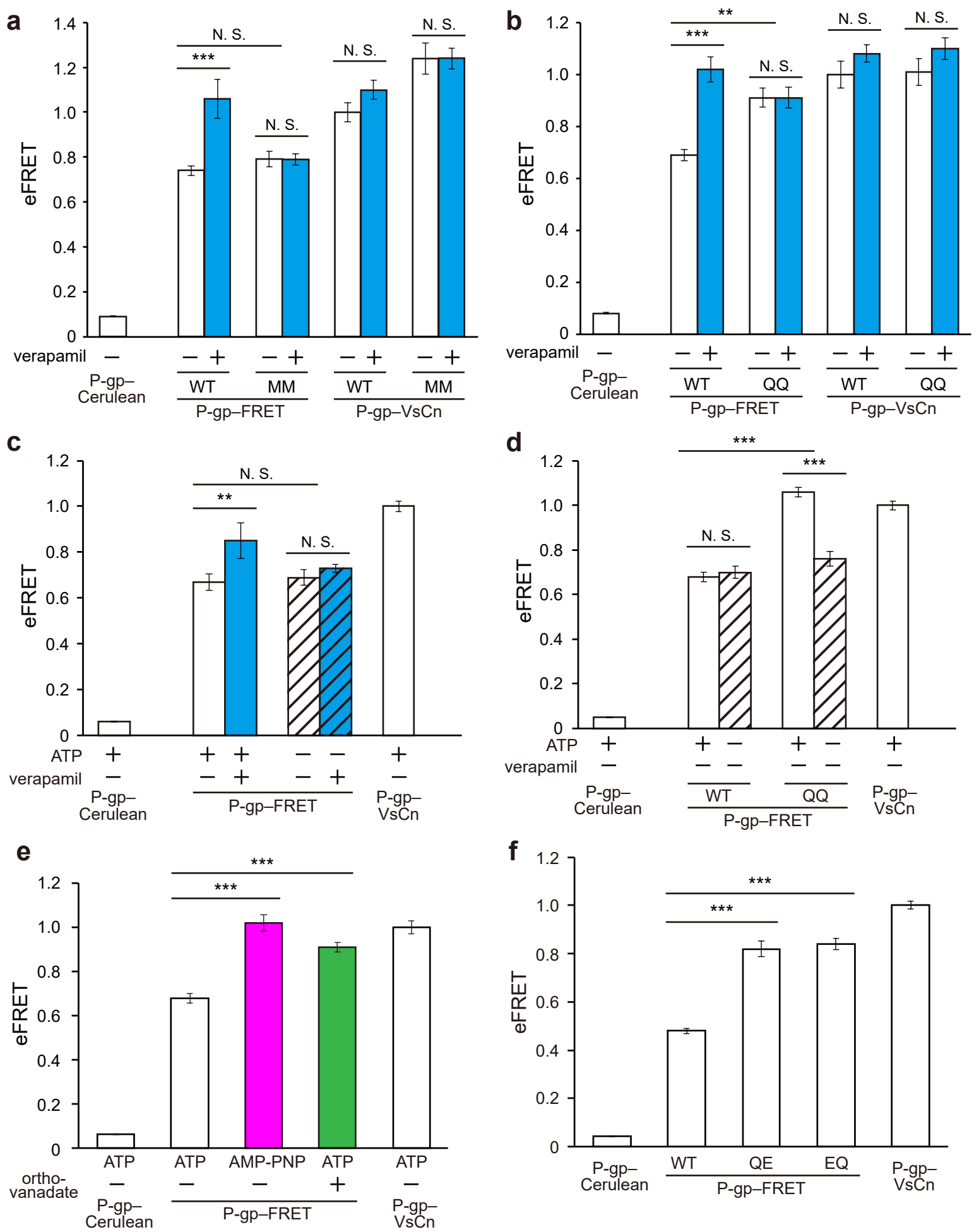
a
eFRET
1.4
1.2
1.0
0.8
0.6
0.4
0.2
0
N. S.
***
N. S.
N. S.
N. S.
verapamil
P-gp–Cerulean
WT
MM
WT
MM
P-gp–FRET
P-gp–VsCn
b
eFRET
1.2
1.0
0.8
0.6
0.4
0.2
0
**
***
N. S.
N. S.
N. S.
verapamil
P-gp–Cerulean
WT
QQ
WT
QQ
P-gp–FRET
P-gp–VsCn
c
eFRET
1.2
1.0
0.8
0.6
0.4
0.2
0
N. S.
**
N. S.
ATP
verapamil
P-gp–Cerulean
P-gp–FRET
P-gp–VsCn
d
eFRET
1.2
1.0
0.8
0.6
0.4
0.2
0
***
***
N. S.
ATP
verapamil
P-gp–Cerulean
WT
QQ
P-gp–FRET
P-gp–VsCn
e
eFRET
1.2
1.0
0.8
0.6
0.4
0.2
0
***
***
ATP
ATP
AMP-PNP
ATP
ATP
ortho-vanadate
P-gp–Cerulean
P-gp–FRET
P-gp–VsCn
f
eFRET
1.2
1.0
0.8
0.6
0.4
0.2
0
***
***
P-gp–Cerulean
WT
QE
EQ
P-gp–FRET
P-gp–VsCn

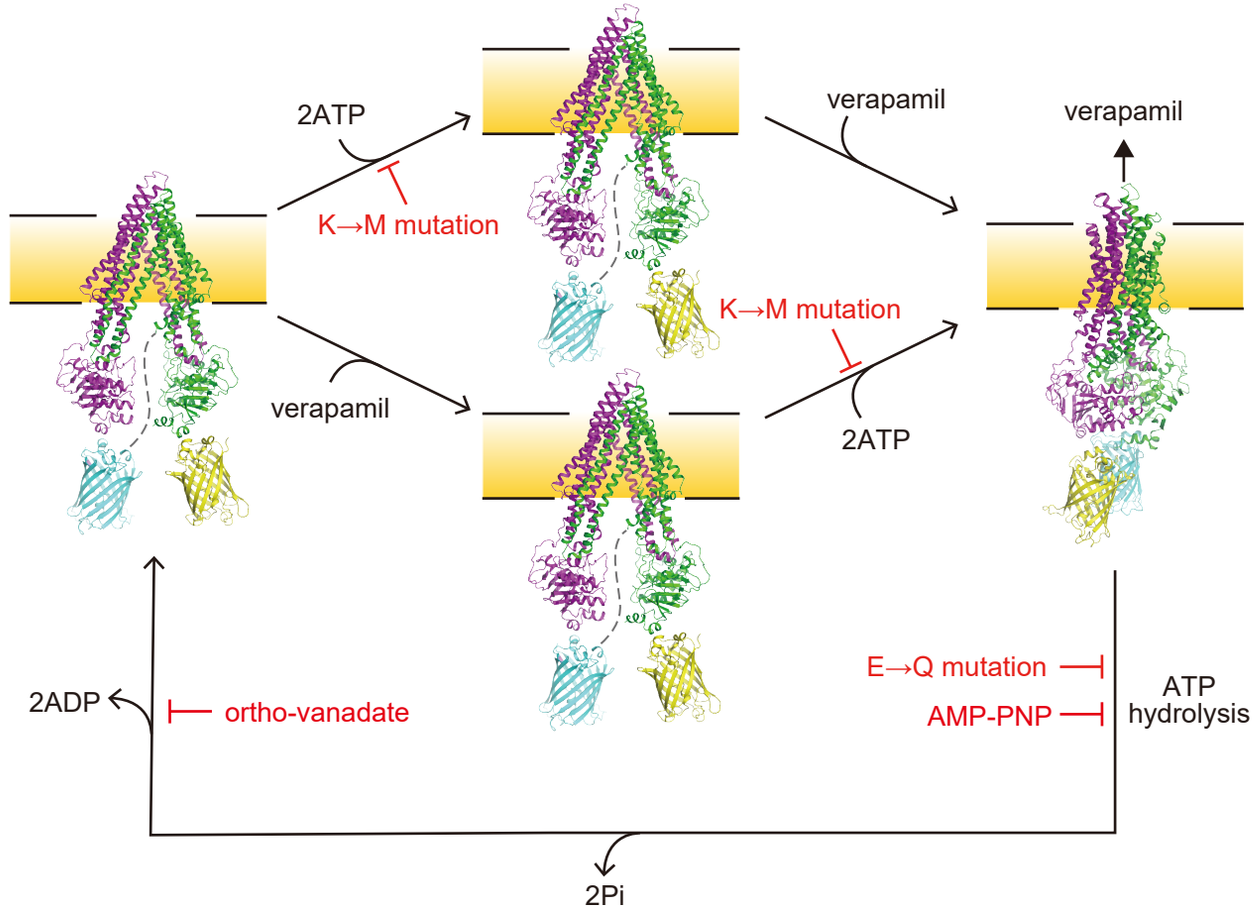
2ATP
K→M mutation
verapamil
verapamil
verapamil
K→M mutation
2ATP
2ADP
ortho-vanadate
E→Q mutation
AMP-PNP
ATP
hydrolysis
2Pi